Supplementary Information for

Aniline-based Hole Transporting Materials for High-Performance Organic Solar Cells with Enhanced Ambient Stability

Tan Ngoc-Lan Phan[†,a], Jinseck Kim[†,a], Geon-U Kim[a], Seungjin Lee[a], and Bumjoon J. Kim[a,]*

[a]Department of Chemical and Biomolecular Engineering, Korea Advanced Institute of Science and Technology (KAIST), Daejeon 34141, Republic of Korea

*Electronic mail: bumjoonkim@kaist.ac.kr

Table of Contents

- **Fig. S12.** Photographs of pH test using pH meter for PEDOT:PSS and PBD:PFBSA (different doping ratios) solutions.

Supplementary Table S1-4

- **Table S1.** PBD:PFBSA film thicknesses and OOP conductances for conductivity calculation.
- **Table S2.** Photovoltaic performance of OSC employing PBD:PFBSA (1:1) as HTL with different solution concentration.
- **Table S3.** Photovoltaic performance of OSC employing PBD:PFBSA (1:1) as HTL with different annealing conditions.
- **Table S4.** Summary of OSC performances employing various aniline-based hole transport layers.

Experimental section

Material Characterizations

^{1}H and ^{19}F nuclear magnetic resonance (NMR) spectra of synthesized PBD and PFBSA were obtained from a Bruker AVANCE III HD Nanobay instrument (^{1}H NMR at 400 MHz, and ^{19}F NMR at 376 MHz) using DMSO-d_6 as solvent. Bruker Autoflex matrix-assisted laser desorption/ionization-time of flight (MALDI-TOF) mass spectrometer or Thermo Fisher Ultimate-3000 ISQ EC liquid chromatograph mass spectrometer were used to measure the molecular weights of synthesized products. Differential scanning calorimetry (DSC) measurements were accomplished by DSC Q200 from TA Instruments (USA) under nitrogen, with both heating and cooling rates of 10 °C min^{-1}. UV–Vis absorption spectra were observed at room temperature by a Shimadzu UV-1800 spectrophotometer. Ultraviolet photoelectron spectroscopy (UPS) and X-ray photoelectron spectroscopy (XPS) measurements were performed on a multipurpose X-Ray photoelectron spectrometer (Thermo VG Scientific). Water contact angle (WCA) measurement was analyzed by contact angle analyzer Phoenix 150 (Surface & Electro Optics Co., Ltd.) using deionized water droplets. Atomic force microscopy (AFM) height images were observed under ambient conditions using a ScanAsyst mode by MultiMode 8 instrument (Bruker). The thickness was obtained from AFM measurement, along with the extrapolation from an absorption-thickness plot in which the absorption probed at 423 nm after the thermal annealing at 90 °C. The pH meter measurements were tested by OHAUS Starter 300 pH meter.

Device Characterizations

The effective area of completed cells was probed by an optical microscopy as 0.164 cm^2. The current density–voltage curves of the devices were quantified by Keithley 2400 SMU Sourcemeter and McScience Inc. K201 LAB55 solar simulator under 100 mW cm^{-2} light irradiation from Xe short-arc lamp provided by the power of 150 W, filtered by a 1.5 G air mass, qualifying the Class AAA of ASTM Standards. The calibration process of light intensity before the measurements was performed employing a McScience Inc. K801S-K302 Si reference cell. EQE spectra of devices were examined by a K3100 IQX instrument (McScience Inc.) using light from a 300 W Xe arc lamp, and MC 200 optical chopper (Thorlabs) under ambient conditions. The obtained J_{SC}s were consistent with the calculated J_{SC}s from EQE spectra within 5% error.

Structural characterization of PBD and PFBSA

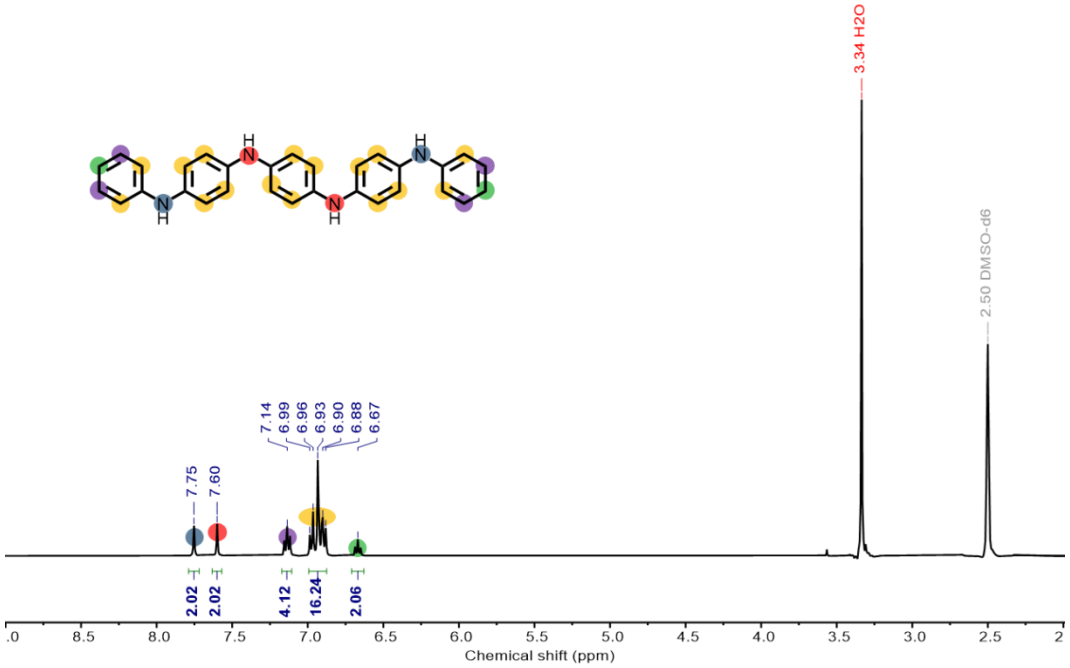

Fig. S1. ^{1}H NMR spectrum of PBD.

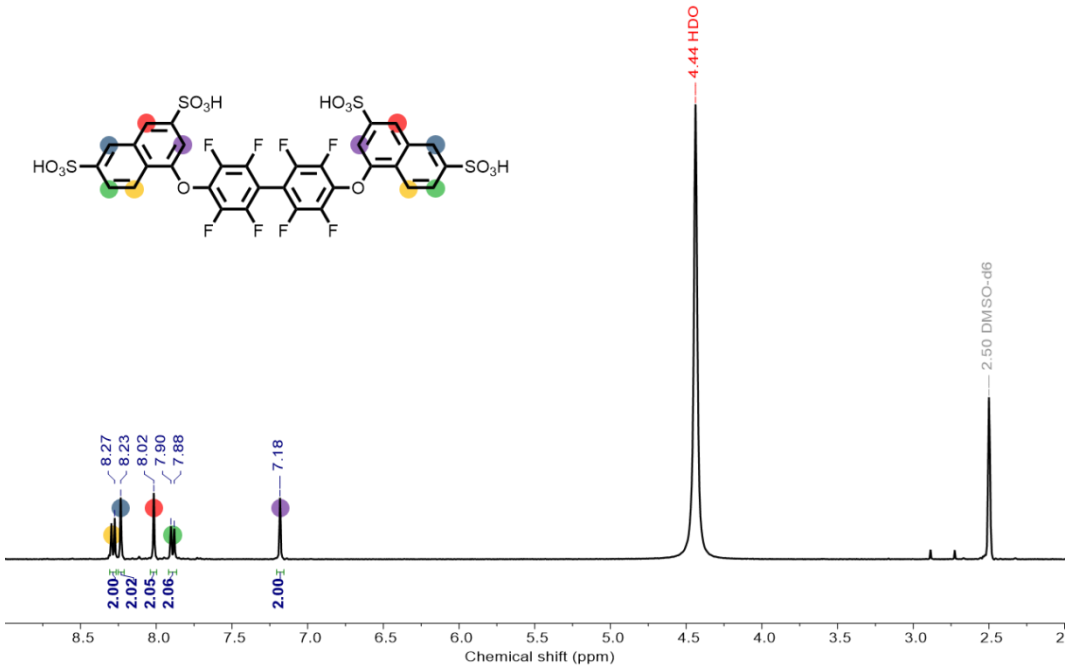

Fig. S2. ^{1}H NMR spectrum of PFBSA.

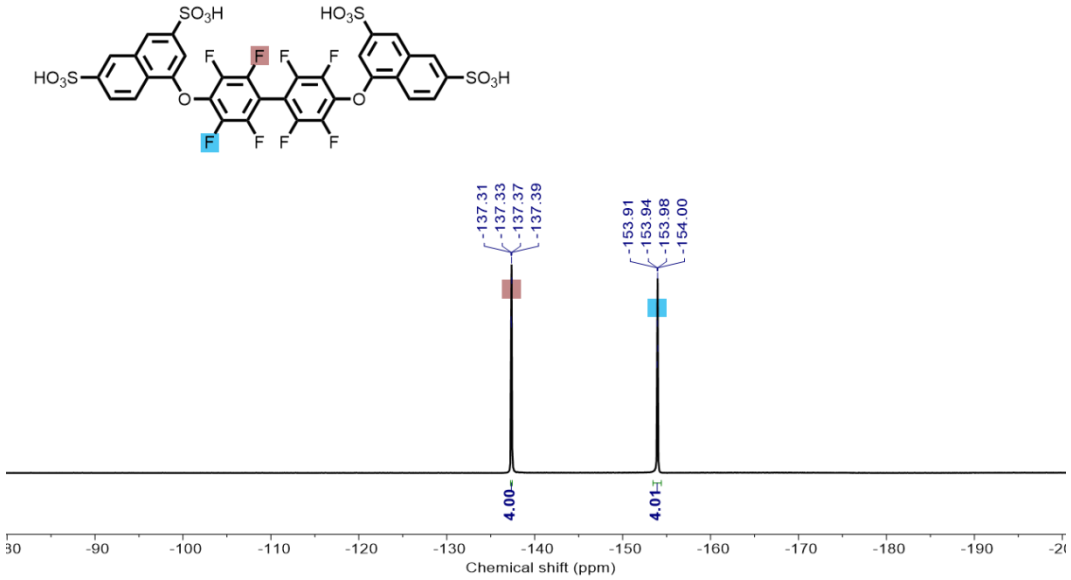

Fig. S3. ^{19}F NMR spectrum of PFBSA.

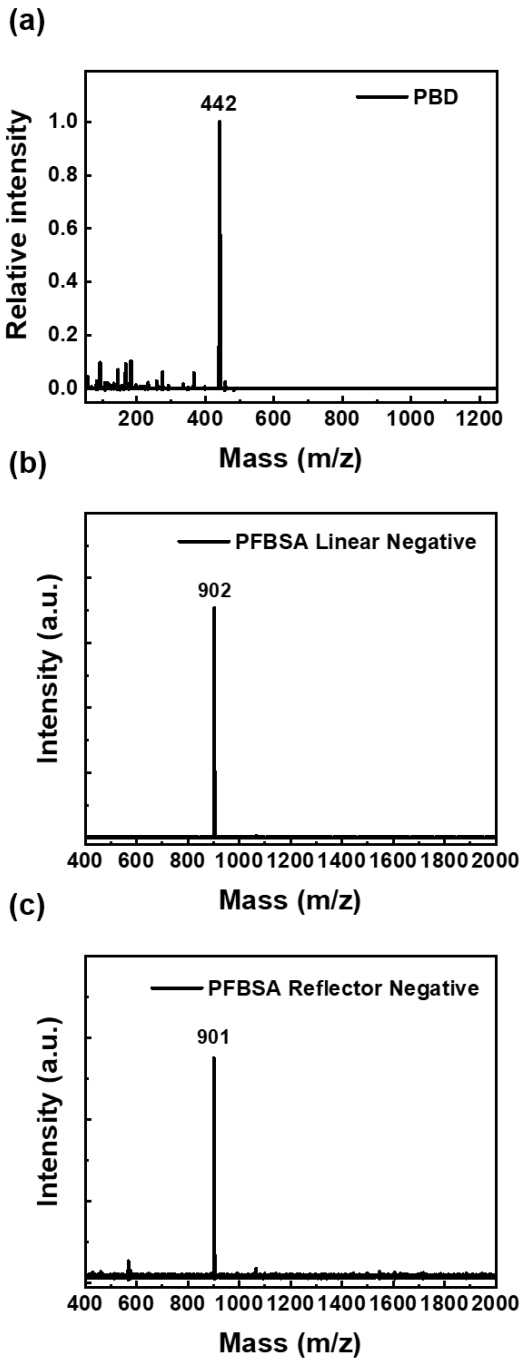

Fig. S4. (a) Mass spectrum of PBD. (b) MALDI-TOF spectra of PFBSA in linear negative mode, and (c) in reflector negative mode.

Crystalline behaviors of PBD, PFBSA, and PBD:PFBSA blends

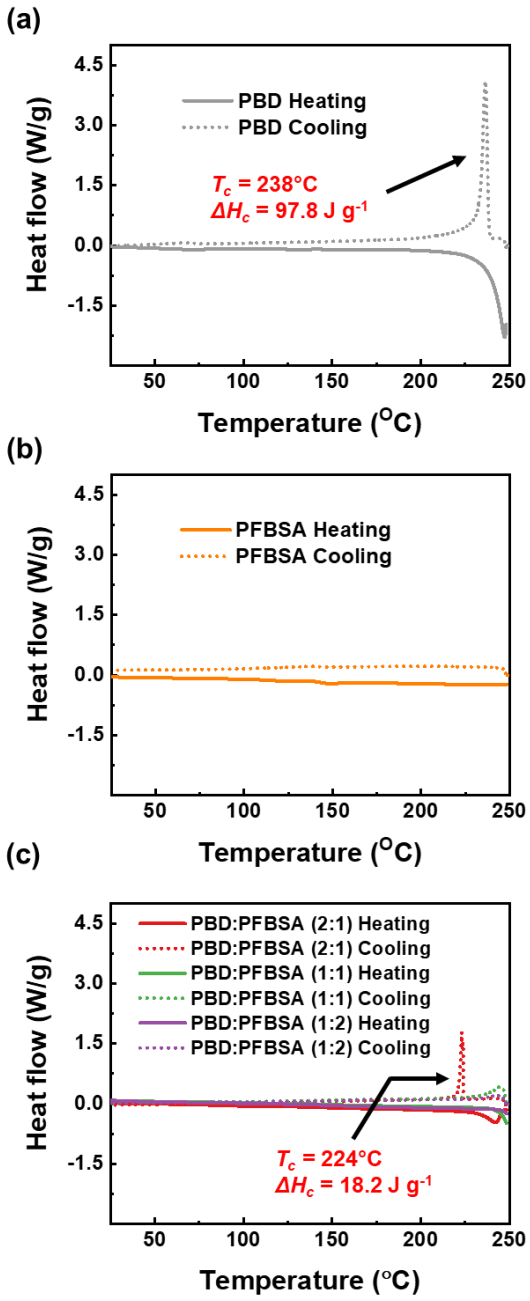

Fig. S5. DSC thermograms during the 1st cooling and 2nd heating cycles of (a) PBD, (b) PFBSA and (c) PBD:PFBSA blends with different doping ratios.

Absorption spectra after annealing process

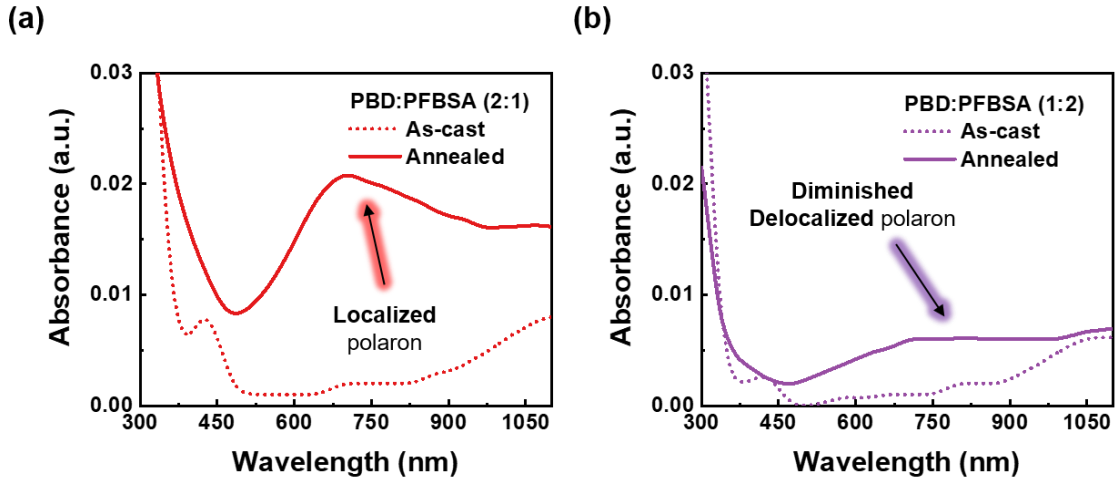

Fig. S6. UV-Vis absorption spectra of as-cast and annealed films from PBD:PFBSA with doping ratios of (a) 2:1 and (b) 1:2.

Work function

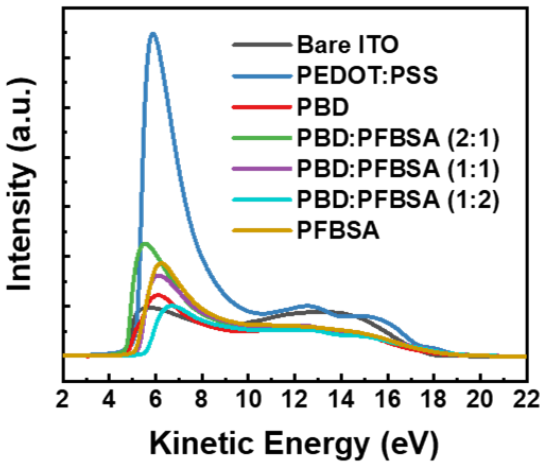

Fig. S7. UPS spectra of the bare ITO, PEDOT:PSS, PBD, PFBSA and PBD:PFBSA (different doping ratios)-coated ITO.

Parameters to calculate out-of-plane conductivity

Table S1. PBD:PFBSA film thicknesses and out-of-plane (OOP) conductances for conductivity calculation.

Material	Doping ratio	Thickness (nm)	Conductance [a] (S)
PEDOT:PSS	1:6	43.5	0.047
PBD:PFBSA	2:1	30.7	0.029
	1:1	30.3	0.101
	1:2	31.6	0.063

[*] Device area of all measured samples is 0.164 cm^2. [a] Determined by the slope of *I-V* curve in the dark.

Solvent orthogonality

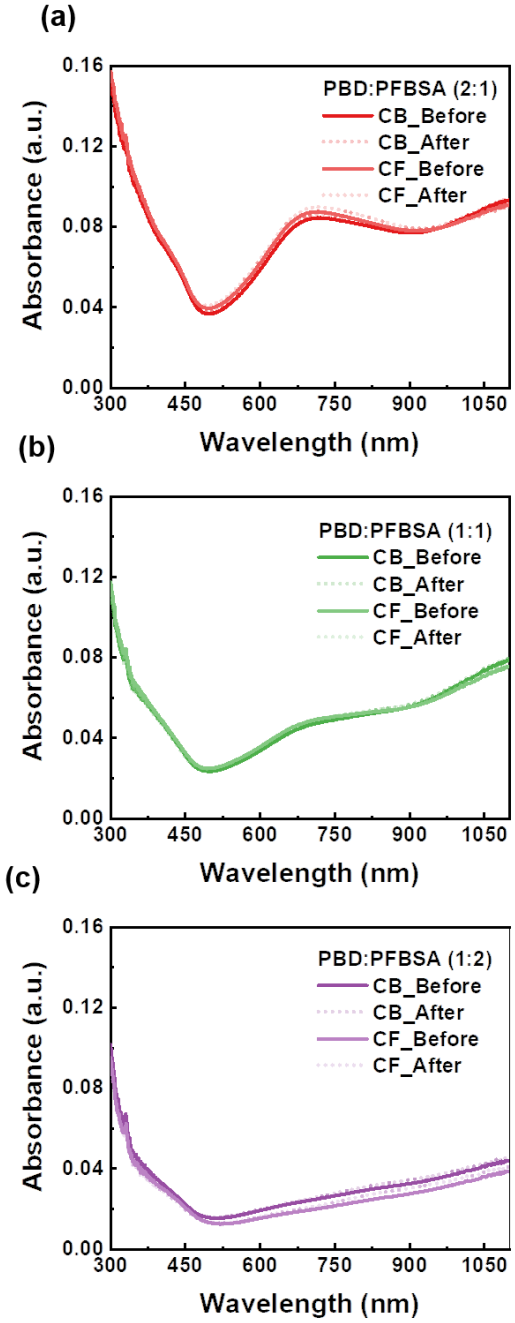

Fig. S8. UV-Vis absorption spectra of the PBD:PFBSA films with doping ratio of (a) 2:1, (b) 1:1 and (c) 1:2, before (solid curves) and after rinsing (short dot curves) with chlorobenzene and chloroform.

Thickness-absorption extrapolation curve

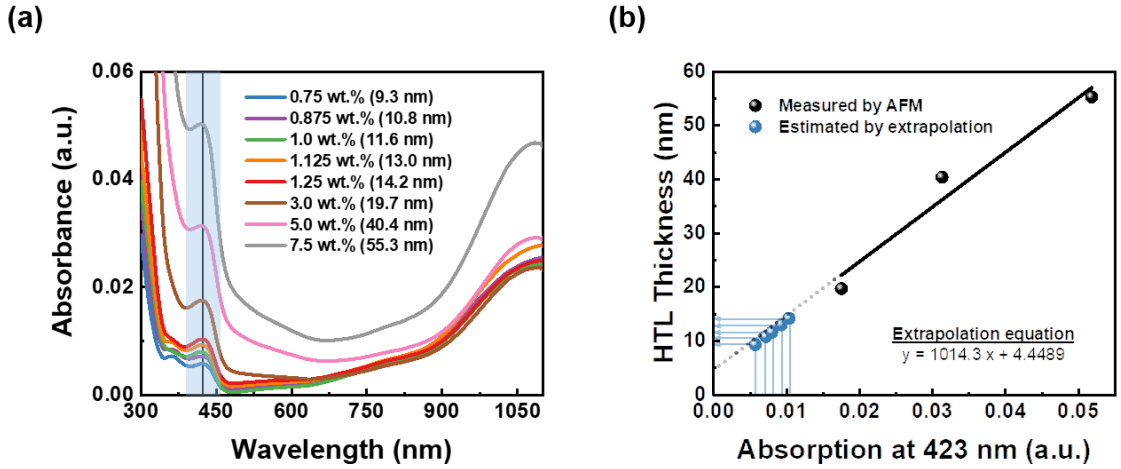

Fig. S9. (a) UV-Vis absorption spectra of PBD:PFBSA (1:1) films after thermal annealing at 90 °C with various thickness controlled by solution concentrations. (b) Extrapolation curve constructed from absorption-thickness relationship of PBD:PFBSA (1:1) films.

Optimization process of OSCs with PM6:Y6 active layer system

Table S2. Photovoltaic performance of OSC employing PBD:PFBSA (1:1) as HTL with different solution concentration. (Processing solvent is DMAc and HTLs were annealed at 250 °C for 10 min).

Concentration (wt/vol %)	Thickness (nm)	V_{OC} (V)	J_{SC} (mA cm^{-2})	FF	PCE (%)
0.75	9.3	0.83	22.12	0.69	12.66
0.875	10.8	0.85	22.65	0.69	13.32
1.0	11.6	0.85	22.86	0.70	13.71
1.125	13.0	0.85	22.18	0.70	13.37
1.25	14.2	0.86	21.63	0.69	12.75

Table S3. Photovoltaic performance of OSC employing PBD:PFBSA (1:1) as HTL with different annealing conditions. (Processing solvent is DMAc and solution concentration is 1.0 wt/vol%).

1st step		2nd step		V_{OC} (V)	J_{SC} (mA cm^{-2})	FF	PCE (%)
Temperature (°C)	Duration (min)	Temperature (°C)	Duration (min)				
-	-	250	10	0.85	22.86	0.70	13.71
90	15	250	5	0.85	23.77	0.71	14.51
90	15	250	10	0.84	25.33	0.72	15.24
90	15	250	20	0.85	24.01	0.68	13.75

Morphology change of ITO modified with PEDOT:PSS and PBD:PFBSA (1:1) HTL

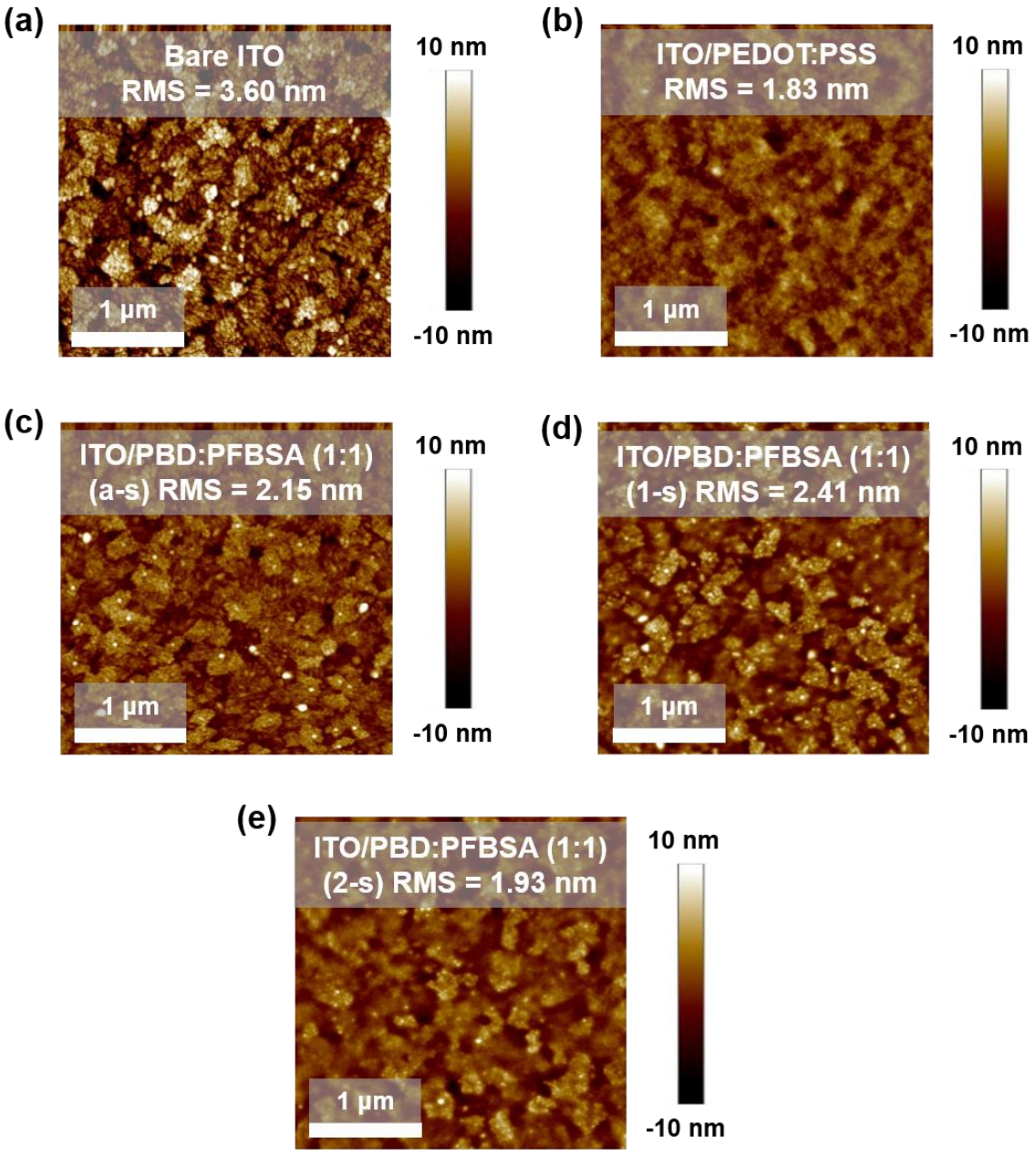

Fig. S10. AFM height images of films from (a) bare ITO, (b) ITO/PEDOT:PSS, ITO/PBD:PFBSA (1:1) (c) as-cast (a-s), (d) after one-step annealing at 250 °C for 10 min (1-s), (e) two-step thermal annealing at 90 °C for 15 min and 250 °C for 10 min (2-s), respectively.

Summary of reported ani-HTLs

Table S4. Summary of OSC performance employing various ani-HTLs

Doping type	Aniline-based HTL	Active layer	PCE (%)	Ref.
Self-doping	SAS10-*gr*-PSSA	P3HT:$PC_{61}BM$	3.42	[1]
	SPAN	P3HT:$PC_{61}BM$	3.54	[2]
	PSSS-*g*-PANI	P3HT:$PC_{61}BM$	3.99	[3]
	PSSA-*g*-PANI/GO	P3HT:$PC_{61}BM$	4.23	[4]
	SPAN(SH)@GNP	P3HT:ICBA	5.19	[5]
	PDAS	PM6:BTP-4F-12	16.2	[6]
Protonic acid doping	PANI:CSA (HP-PANI)	P3HT:$PC_{61}BM$	1.3	[7]
	PANI/PEDOT:PSS	P3HT:$PC_{61}BM$	2.76	[8]
	PANI:PSS (1:1.5)	P3HT:ICBA	3.5	[9]
	HAPAN	P3HT:$PC_{71}BM$	3.70	[10]
	PANI:PSS (1:0.5)	P3HT:ICBA	4.0	[9]
	PANI:PSS (1:1)	P3HT:ICBA	4.5	[9]
	HAPAN	PBTTDPP-T:$PC_{71}BM$	5.99	[10]
		PDPP3T:$PC_{71}BM$	7.13	[10]
		PBDTBDD:$PC_{71}BM$	7.20	[10]
		PTB7:$PC_{71}BM$	7.64	[10]
		PBDTTT-C-T:$PC_{71}BM$	7.71	[10]
		PBDTTT-EFT:$PC_{71}BM$	9.05	[10]
	PBD:PFBSA (1:1)	PM6:Y6	15.24	This work

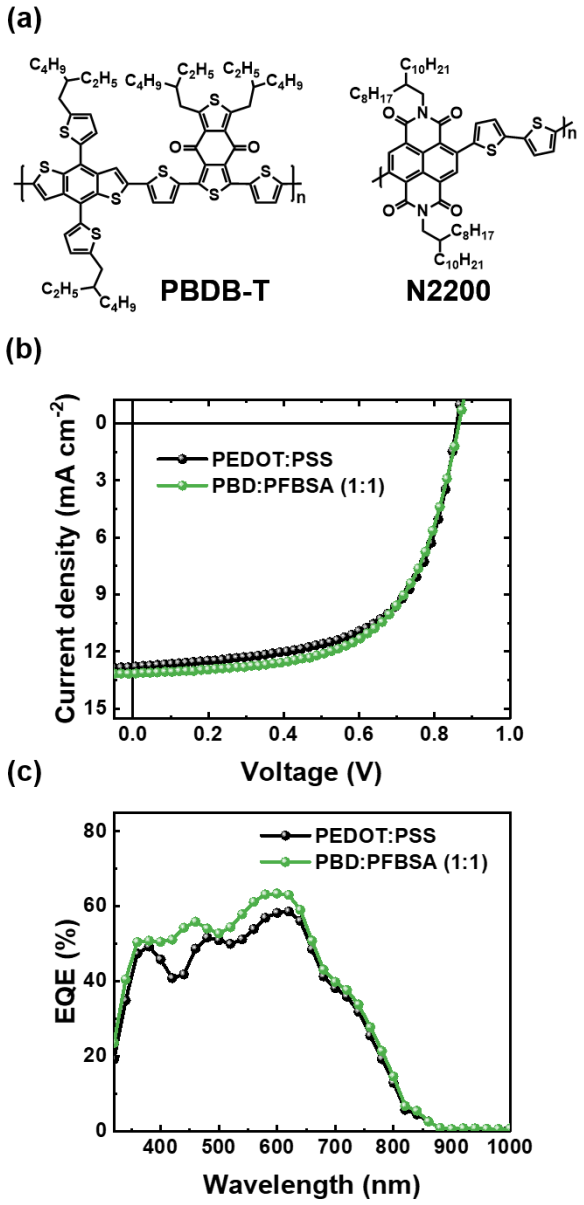

Fig. S11. (a) Chemical structure of PBDB-T and N2200 active layer materials used in versatility study. (b) *J*-*V* curves and (c) EQE curves of the OSC devices fabricated with PEDOT:PSS and PBD:PFBSA (1:1).

pH measurement

Fig. S12. Photographs of pH test using pH meter for PEDOT:PSS and PBD:PFBSA (different doping ratios) solutions.

References

1 T. H. Lim, K. W. Oh and S. H. Kim, *Synth. Met.*, 2012, **162**, 268-275.

2 W.-J. Ke, G.-H. Lin, C.-P. Hsu, C.-M. Chen, Y.-S. Cheng, T.-H. Jen and S.-A. Chen, *J. Mater. Chem.*, 2011, **21**, 13483-13489.

3 J. W. Jung, J. U. Lee and W. H. Jo, *J. Phys. Chem. C*, 2010, **114**, 633-637.

4 S. Bae, J. U. Lee, H.-s. Park, E. H. Jung, J. W. Jung and W. H. Jo, *Sol. Energy Mater. Sol. Cells*, 2014, **130**, 599-604.

5 S.-A. Gopalan, A.-I. Gopalan, A. Vinu, K.-P. Lee and S.-W. Kang, *Sol. Energy Mater. Sol. Cells*, 2018, **174**, 112-123.

6 M. Zeng, W. Zhu, J. Luo, N. Song, Y. Li, Z. Chen, Y. Zhang, Z. Wang, W. Liang, B. Guo, K. Zhang, F. Huang and Y. Cao, *Sol. RRL*, 2021, **5**, 2000625.

7 O. Abdulrazzaq, S. E. Bourdo, V. Saini, V. G. Bairi, E. Dervishi , T. Viswanathan, Z. A. Nima and A. S. Biris, *Energy Technol.*, 2013, **1**, 463-470.

8 Y.-K. Han, M.-Y. Chang, K.-S. Ho, T.-H. Hsieh, J.-L. Tsai and P.-C. Huang, *Sol. Energy Mater. Sol. Cells*, 2014, **128**, 198-203.

9 S. Biswas, Y.-J. You, J. Kim, S. R. Ha, H. Choi, S.-H. Kwon, K.-K. Kim, J. W. Shim and H. Kim, *Appl. Surf. Sci.*, 2020, **512**, 145700.

10 W. Zhao, L. Ye, S. Zhang, B. Fan, M. Sun and J. Hou, *Sci. Rep.*, 2014, **4**, 6570.